Experimental evaluation of heat transfer performance under natural and forced convection around a phase change material encapsulated in various shapes

Xiaolin Wang[a,*], Una Djakovic[a], Huashan Bao[b], Juan F. Torres[a]

a Research School of Electrical, Energy and Materials Engineering, The Australian National University, Canberra, ACT 2601, Australia

b Department of Engineering, Durham University, Durham, UK, DH1 3LE

*Corresponding authors: xiaolin.wang@anu.edu.au

Abstract: Cold thermal energy storage can reduce peak electricity use in electric air conditioning systems as well as improve free space cooling, through convective heat transfer between a surrounding fluid (heat transfer fluid or air) and encapsulated phase change material (PCM). In this work, heat transfer performances and phase change behaviours of six PCM capsules with equal-volumes but varying-shapes were studied experimentally, for use in cold latent heat storage. A tetra-*n*-butylammonium bromide-based PCM with an adjustable phase change temperature of 0–12°C was injected into capsules of spherical, cylindrical (short and long), pyramidal, tetrahedral, and a biomimetic red blood cell shape. First, an infrared camera recorded the surface temperature variation during the melting process of each capsule in air under natural convection. Second, an experimental setup was built to investigate latent heat storage during the freezing and melting processes for each shape under forced convection, focusing on the effects of fluid temperature, flowrate and PCM capsule tilt angle on freezing and melting times. The results showed that the freezing and melting time was dependent on not only the surface area to volume ratio, but also on the distance from centroid to inner capsule surface. Importantly, the red blood cell shape was found to be the most favourable geometry because it yielded the most rapid freezing and melting process, which were further enhanced in a configuration where the freestream flow directly impinged onto its centroid. The work is a pioneering study on the PCM capsule geometry topic that provides experimental data and recommendations for future studies and applications.

Keywords: capsule geometry; cold thermal storage; natural convection; forced convection

1 Introduction

In recent years, the energy used in temperature regulation of commercial and residential buildings has shown significant growth in the share of the overall energy consumption and CO_2 emissions produced [1]. The large and growing energy demands, especially for cooling, have had significant economic and environmental effects, such as a lack of energy resources to allow for economic development as well as an increased use of fossil fuels contributing to climate change [1]. One such method, cold thermal energy storage (CTES) accumulates cold thermal energy by cooling a storage medium so that the stored energy can be later used for cooling applications [2]. It offers an effective way to mitigate peak electricity demand by shifting the electricity use for running the chiller to off-peak periods. Reducing power consumption during peak periods alleviates the grip pressure, secures the grip safety, and enables greater usage of excess electricity generation from renewables [3, 4]. For example, for solar thermal cooling, it helps alleviate the effects of solar intermittency, where excess harvested solar energy can be used to drive the chiller and cool the storage medium, allowing for later cooling release at times of solar outage [5–7].

CTES, particularly the use of phase change materials (PCMs) as the medium, has in recent years become popular due to its small footprint, scalability, and simple modification of existing cooling systems [8–11], making the implementation of CTES systems cheaper, easier and more versatile. At present, PCM-based CTES in buildings mainly has two application approaches. The conventional approach relates to a packed-bed CTES with encapsulated PCM [12]. Here, the CTES system is usually placed in parallel to the air conditioning (AC) chiller and the cooling load (AC users) with a heat transfer fluid (HTF) to carry and exchange cooling capacity. Numerous capsules containing PCM are generally used instead of a large lump of PCM to increase the heat transfer area, as the PCMs have generally low thermal conductivity. Sphere is the conventional and most popular shape of PCM capsules for the convenience in fabrication. Another approach is

to embed PCM in building envelops, such as walls, roofs, and ceilings [13, 14]. Higher thermal mass of building materials leads to less temperature fluctuation and energy consumption of the building for heating and cooling. However, thermal mass of building has been largely reduced due to the development of construction technology and lighter building materials [15]. PCM in building envelops can help with the thermal management in buildings due to its large energy storage density and small temperature change during charging/discharging of thermal energy. A widely used configuration is to sandwich a PCM layer (PCM encapsulated in a flat plate) into the wallboard and insulation layers.

For most applications, rapid charging and discharging processes are desirable, as a high charging rate results in a short charging time and a high discharging rate allows for a large cooling capacity supply in order to meet the desired cooling load. Heat transfer performance under various conditions, e.g. natural convection and forced convection, is a determining factor of the charging and discharging rate of thermal storage systems. However, neither the spherical PCM capsule in CTES nor the plane PCM-embedded panel in walls has been proven efficient in their heat transfer performance. In fact, capsule shape does have a significant impact on its heat transfer performance, as in structures of different shapes surrounded by an air/liquid flow and undergoing mixed convection [16, 17].

Numerous studies have been conducted on capsules and improving their thermal transfer properties to achieve a decreased charging time. Chandrasekaran et al. [10] experimentally investigated the effect of spherical capsule size on its charging characteristics. Deionized water was used as the PCM, and stainless-steel capsules were submerged in an insulated thermostatic bath with freestream temperature ranging from –6 to –12°C. A shorter freezing time was found for larger capsules up until 75% solidification with a lower solidification rate for the remaining 25%, owing to the higher thermal resistance near the centre of the PCM. Studies of more complex modifications to spherical capsules have been conducted. Jia et al. [8] conducted a thermal performance analysis of aluminium alloy spherical capsules with interior pin-fins for enhanced thermal conduction. Data was obtained via simulation and experiment, considering varied pin-fin number, diameter and length. Their study showed a negative correlation between charging time and pin-fin number, and a decrease in charging time of up to 59.74% for the same sized capsule with and without six pin-fins. To study the effects of capsule material, ElGhnam et al. used capsules made of copper, brass, glass, plastic and stainless steel to test charging and discharging times [18]. The copper capsule resulted in the shortest while the plastic one showed the longest freezing and melting times. However, the decrease in charging and discharging times with the use of the copper capsule was deemed quite small. A similar experimental study conducted by Reddy et al. [19] showed consistent results. Three capsule materials were used (plastic, aluminium and steel) and the charging and discharging times varied up to only approx. 5% among them. This small variation once again proved that the effect of capsule material was not significant. Both studies suggested that changing the material is not a cost-effective way to improve PCM capsule performance. The influence of HTF temperature and flowrate were also investigated. Benmoussa et al. [20] investigated the effects of HTF inlet temperature on the melting of two PCMs in a cylindrical annulus capsule through simulation. A general trend of decreasing melting time with an increasing inlet temperature was observed. Cheng et al. [21] found that a higher HTF mass flowrate resulted in a lower charging time, with the difference in charging times decreasing with each increase in flowrate.

Increasing the surface area to volume (SA/V) ratios of the capsules by modifying their shape is another method to increase the heat transfer between the encapsulated PCM and its surroundings [22]. Although spherical capsules have been the focus of most studies, capsules of other shapes with differing SA/V ratios have also been investigated. Darzi et al. [23] conducted numerical simulations of capsules in the shape of cylindrical annuli. Theoretical modifications were conducted including an elliptical inner tube instead of circular, and the addition of radial conductive fins. For a given volume, an ellipse will have a greater circumference, meaning the overall surface area of elliptical annulus is greater, i.e. a greater SA/V ratio. The results showed a comparatively lower melting time for the vertically oriented ellipse of the annulus, however the charging time was deemed very inefficient for this configuration. Awasthi et al [24] investigated the melting characteristics of a cylindrical capsule with a sinusoidal capsule surface, varying the sinusoid

amplitudes and frequencies. Maintaining the capsule cross-sectional area constant, while increasing its circumference (increasing the SA/V ratio) through a larger sinusoid amplitude, showed a decrease in melting time. Cheng [22] studied the thermal performance of a PCM capsule in red blood cell (RBC) shape via experiment and simulation. Due to its biconcave disc shape, the RBC has a large SA/V ratio. Through a direct comparison with a spherical capsule, a charging rate of 2.12 times that of the spherical capsule for the RBC capsule was observed. Optimizations of geometrical parameters were also conducted through simulation and the dimension ratios equal to that of a human RBC were found to be optimal. This study, however, did not investigate the melting rate of capsules, an equally important factor that determines PCM capsules' efficacy. Additionally, one thermocouple was placed in each capsule at its geometric centre, which is not representative of the temperature distribution inside the PCM. The melting characteristics in a horizontal cylindrical capsule were investigated by Hlimi et al. [25] through numerical modelling, finding that early stages of melting were mostly based on conduction, whereas later stages were driven by convection caused by the buoyancy of the solid PCM remaining in its melted portion.

Factors on PCM capsule heat transfer performance such as PCM properties and operational conditions have been extensively researched previously. However, the effect of capsule geometry, specifically unfrequently used shapes, on the heat transfer properties and performance of the PCM capsule has not been disclosed, despite their very high SA/V ratios compared to spheres. As a result, there is a significant lack of studies on the thermal performances of capsules having various non-spherical shapes. In addition, a number of numerical studies conducted on PCM capsules in CTES and their influencing factors have been found, however not enough experimental data is provided to evaluate the reliability of simulation results.

This study aims to experimentally explore new shapes of PCM capsules, namely cylindrical, RBC, tetrahedral and pyramidal shapes, focusing on their heat transfer properties and PCM phase change behaviour under natural and forced heat convection regimes. A one-on-one comparison is conducted on capsules in various shapes with the widely used spherical capsule, with equal wall thicknesses and inner volume, in order to identify the capsule shape with the best heat transfer performance. In addition, the influencing factors of the capsules are investigated including the HTF flowrate, HTF temperature and capsule tilt angle relative to the main flow. PCM capsules are applied in CTES through convective heat transfer between a surrounding fluid (HTF or air) and encapsulated PCM. Therefore, potential applications of this results of this study are illustrated in Figure 1 for PCM-embedded panels (heat transfer with air) and Figure 2 for PCM packed-bed CTES (heat transfer with HTF), with different PCM capsule geometries.

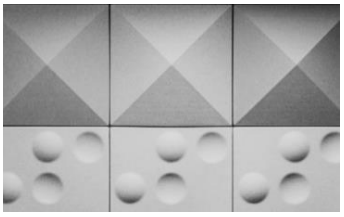

Figure 1. Indicative schematic of building wall or ceiling panels with PCM capsules in different shapes [26].

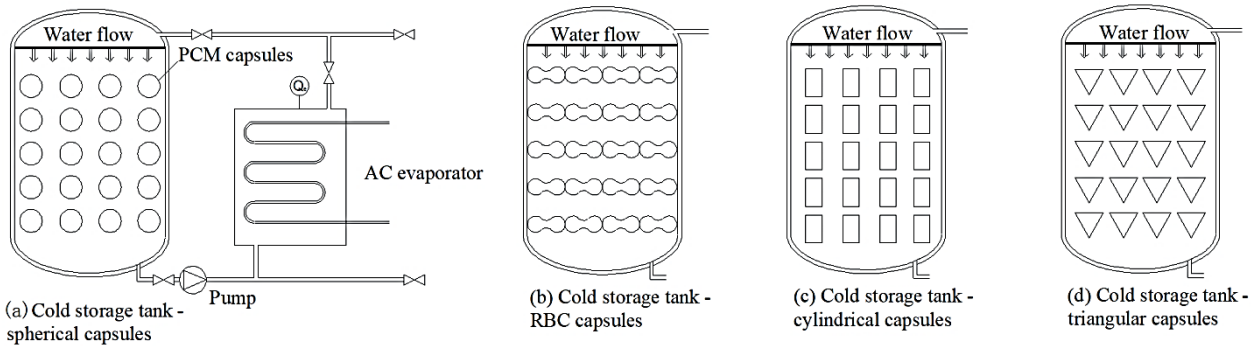

Figure 2. Indicative schematic of packed-bed CTES with PCM capsules in different shapes.

2 Experimental setup and procedures

2.1 Phase change material

The PCM employed in this study is tetra-*n*-butylammonium bromide (TBAB), a quaternary ammonium salt with a bromide counter ion, the aqueous solution which can form a clathrate hydrate. TBAB clathrate hydrate has been widely used for CTES applications due to its suitable phase change temperature range for various cooling applications (from 0 to 12°C) by adjusting the concentration of TBAB in the solution. It has been reported in a number studies, including experimental demonstrations [12, 27–29] and practical systems [30]. The prepared PCM, whose thermal properties are listed in Table 1, was injected into capsules of different shapes.

Table 1. Thermal properties of tetra-*n*-butylammonium bromide, the phase change material in this study.

Composition	Density (kg m^{-3}) [31]	Phase change temperature (°C)	Enthalpy (kJ kg^{-1}) [31–33]	Thermal conductivity (W $m^{-1}K^{-1}$) [34]	Quantity of PCM in capsules (g)
TBAB 40 wt% in water	1030–1082	12.8	193.2–210.0	0.380–0.388	14.5

The phase change temperature was measured using a differential scanning calorimeter. The repeatability of phase change of the PCM was examined via ten continuous cooling and heating cycles, and a small variation of 1.60% of phase change temperature was measured. An in-depth analysis of pure TBAB power and its 40 wt% water solution of TBAB using Fourier-transform infrared spectroscopy was conducted in a cell with optical path of 10 mm, as shown in Figure 3. The peaks in the curve of pure TBAB at 2876 cm^{-1} indicate C–H bonds of butyls, and the large peak in the curve of water solution of TBAB at 3369 cm^{-1} indicates O–H bonds of water.

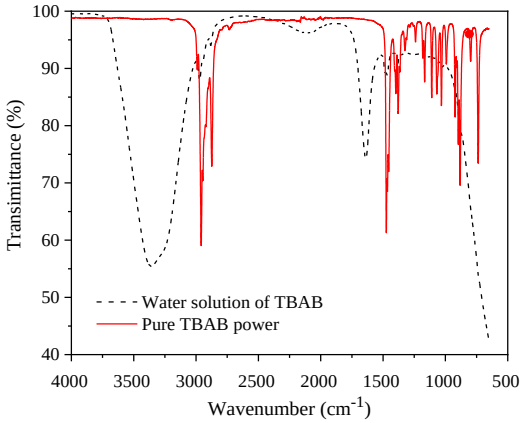

Figure 3. Fourier-transform infrared spectroscopy analysis of TBAB (solid line) and the PCM composed of TBAB and water (dashed line).

2.2 PCM capsules

Six capsules were 3D-printed using high-transparent resin (Crysta-8) as the shell material. A photograph of the capsules is shown in Figure 4. The capsules were fabricated with the same internal volume of 15 mL and a shell thickness of 1 mm. Table 2 lists the important geometric properties of inner SA/V ratio, outer surface area and characteristic dimension of the six capsules. The RBC-shaped capsule follows an optimised geometry (the ratio of thickness at the centre to disk diameter) based on the study of Cheng et al. [21]. Three thermocouples were inserted in each capsule at varying positions along their central axis, i.e. 1/4, 1/2 and 3/4 of the internal height as the distance from the top, to investigate the temperature distribution, enabling a better understanding of the solidification and melting process of the encapsulated PCM. The properties of Crysta-8 material are shown in Table 3 (data from the manufacturer).

Table 2. Geometrical parameters of PCM capsules.

	Sphere	Tall cylinder	Short cylinder	Tetrahedron	Pyramid	RBC
Inner SA/V ratio (m^{-1})	0.22	0.26	0.26	0.36	0.34	0.27

Outer surface area ($\times 10^{-3}$ m^2)	3.34	4.21	4.23	5.47	5.12	4.01
Distance from surface to centroid (mm)	15.3	10.8–24.1	8.55–20.0	14.0–28.0	9.96–29.2	8.11–11.1

Table 3. Mechanical properties of Crysta-8 capsule shell.

Critical exposure energy (MJ cm^{-2})	Tensile modulus (kPa)	Tensile strength (MPa)	Elongation at break (%)	Thermal deflection temperature (°C)
6.7	2.58–2.67	45–60	6–10	55–67

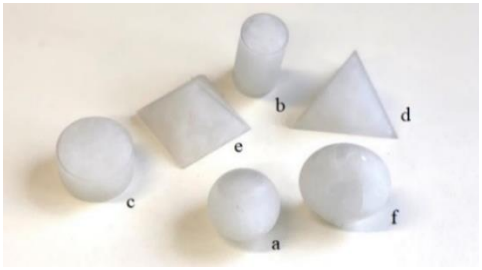

Figure 4. 3D-printed capsules containing solid PCM, with the shape of (a) sphere, (b) tall cylinder, (c) short cylinder, (d) tetrahedron, (e) pyramid and (f) RBC.

2.3 Experimental setup and procedure

The experiment was composed of two stages. The first stage evaluates the heat transfer performance of PCM in building envelopes with natural convection and surrounding air at 23°C, focusing on the melting characteristics. The second stage evaluates the heat transfer performance of the PCM capsule in CTES under forced convection with a 20% wt. propylene glycol and water solution. In the first stage, a series of infrared (IR) images of the PCM capsules were taken using an IR camera with a time interval of 5 min. The IR camera was FLIR T640 with an accuracy of ±2°C (±3.6°F) or 2% at 25°C (77°F) nominal, and a resolution of 640 × 480 pixels. The emissivity of capsule material used in the IR camera was calibrated by direct measurements with thermocouples. Together with the IR images, a temporal evolution of the temperature inside the PCM was recorded.

In the second stage, a testing system was assembled to conduct the testing of the capsules exposed to a flowing HTF. A cylindrical HTF tunnel (300 mm in length and 150 mm in diameter) with an inlet and outlet, as shown in Figure 5(a), was connected to a thermostatic bath with circulation capabilities through PVC piping, as indicated in Figure 5(b). Valves were used to enable the control of HTF flowrate in and out of the tunnel. Thermocouples were placed at various positions in the system and connected to a data logger (DataTaker DT80). In addition to the three thermocouples placed in the inside of the capsule at the equant top, middle and bottom positions, two thermocouples (*front* and *rear*) were placed next to the inlet and outlet inside the container, and two (*in* and *out*) were placed in the inlet and outlet piping, as shown in Figures 5(b). The accuracy of the K type thermocouples is (whichever is greater): ±2.2°C or ±0.75%. To begin the solidification process, an HTF temperature lower than the freezing point was used to overcome supercooling and to create a sufficient temperature difference between the PCM and the HTF. Once the PCM was deemed completely solidified by both temperature and visual inspections, the thermostatic bath temperature was increased to initiate the melting. The temperatures were recorded until all PCM melted.

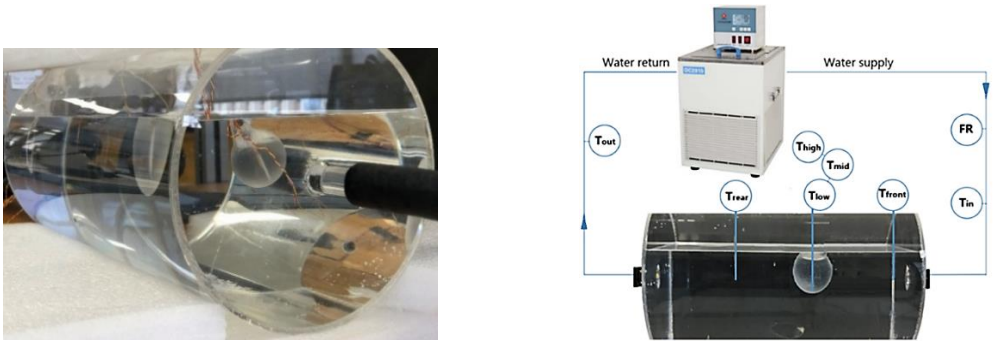

(a) (b)

Figure 5 Experimental setup with a single PCM capsule: (a) HTF tunnel and (b) experimental testing system.

4 Result and discussions

4.1 Melting of PCM capsule with different shapes under natural convection

To study the melting process of PCM capsules in different shapes under natural convection in ambient air, IR images were taken based on a temperature scale of 0–25.9°C, as shown in Table 4, with the capsule size (see Table 2) serving as the scale of the images. The IR images were processed for temperature variation at three fixed positions on the capsule surface, as shown in Figure 6.

The temperature profiles in Table 4 suggest that all capsules started melting from the top, possibly due to a thinner boundary layer developing from the top surface of the capsule. The melting process is expected to occur throughout the shell-PCM boundary, so persisting low temperatures at the bottom suggest that the PCM solid core in the centre moved downwards due to its higher density than liquid PCM. At 165 min, the surface temperature of the PCM capsule in tetrahedron shape was the closest to that of the ambient, which is expected due to its largest SA/V ratio, followed by pyramid and tall cylinder. However, the completion of the melting process of the six capsules (revealed by a rapid temperature increase after the temperature platform for all the three temperature curves), as indicated by the dash vertical lines in Figure 6, was about 139 min for tetrahedron, 131 min for pyramid, 140 min for tall cylinder, 149 min for short cylinder, 130 min for RBC and 150 min for sphere. The RBC-shaped and pyramid-shaped capsules had better performance. In contrast, the spherical and short cylinder-shaped PCM capsules took the longest to complete melting.

It was also speculated that a longer vertical dimension (in the gravity direction) of a capsule is beneficial to the natural convection of the internal PCM during melting. As a longer travel distance can be provided by a capsules longer vertical dimension, the sedimentation of the solid core may assist to intensify the natural convection and unify the temperature in the capsule, thus accelerating the melting process.

Table 4. Infrared camera images of capsules during melting in natural convection with air.

Time for cooling	Sphere	Tall cylinder	Short cylinder	Tetrahedron	Pyramid	RBC	
15 min	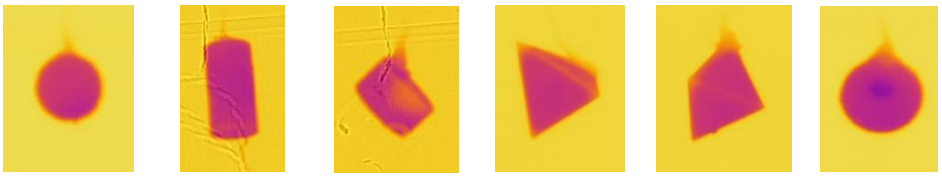						
90 min	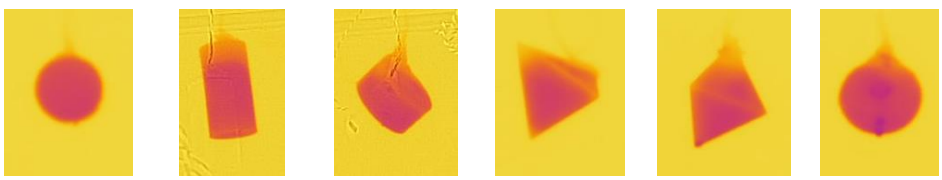						

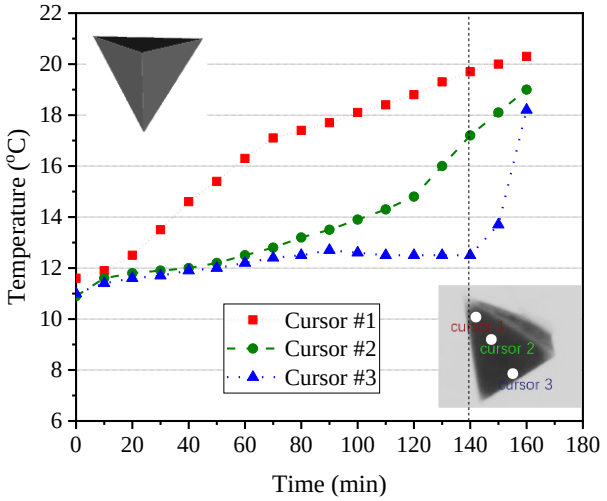

(a) Tetrahedron

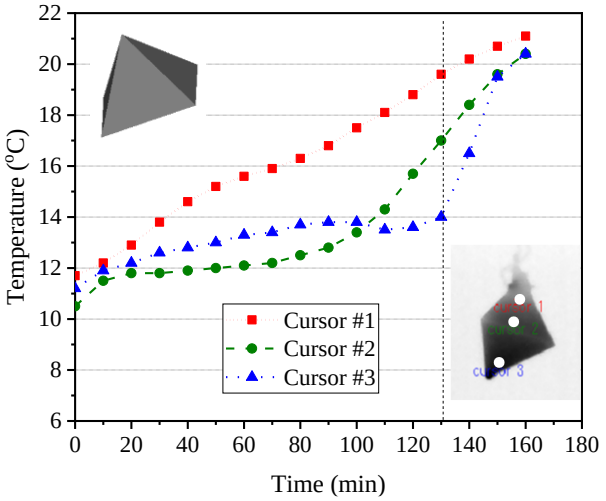

(b) Pyramid

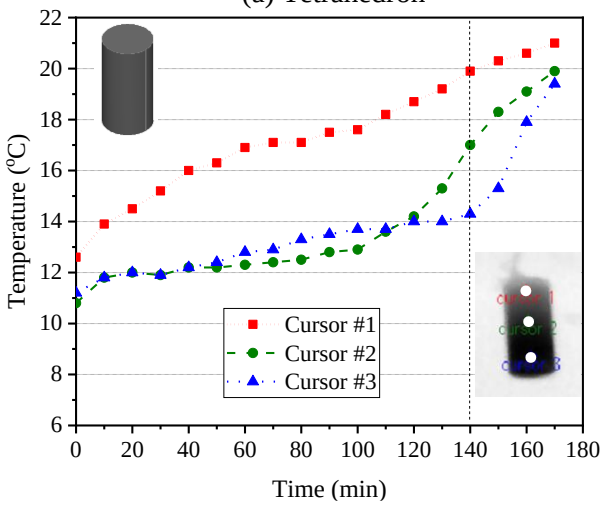

(c) Tall cylinder

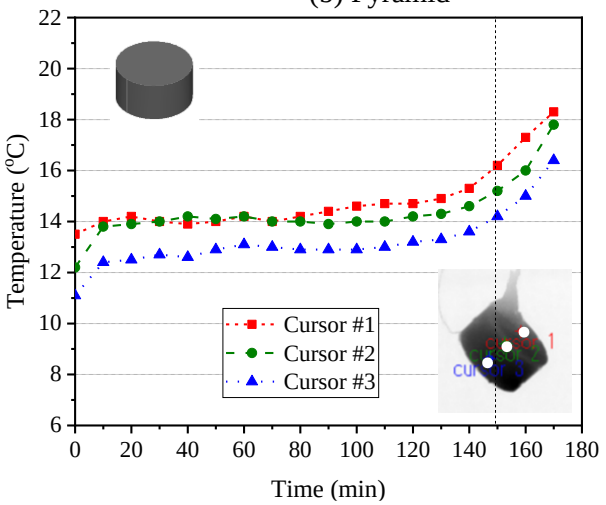

(d) Short cylinder

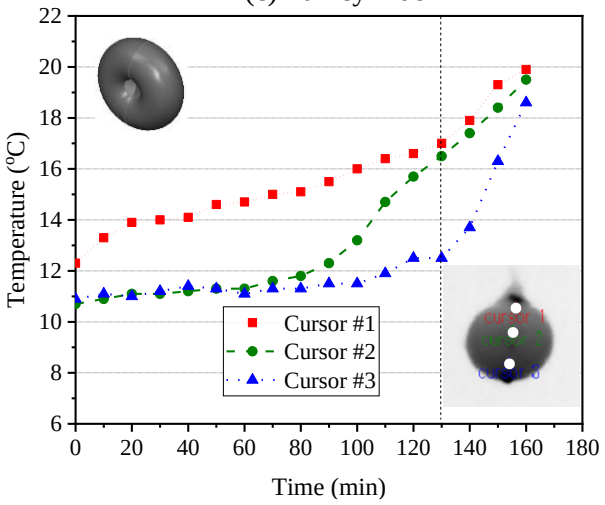

(e) RBC

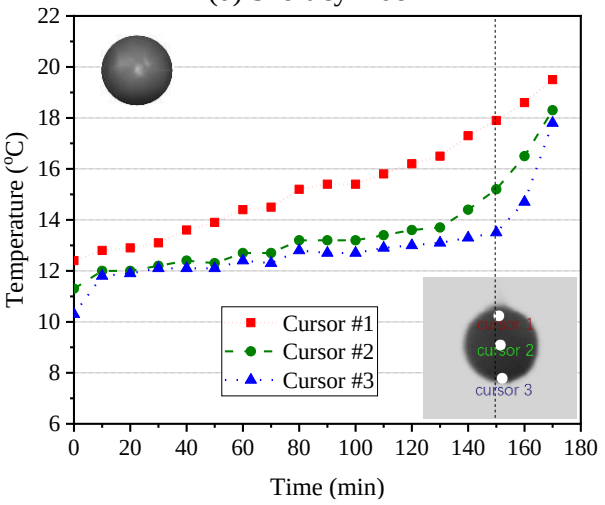

(f) Sphere

Figure 6. Capsule surface temperature variation during melting.

4.2 Melting and freezing of PCM capsules under forced convection

To study forced convection, the experiments were firstly operated at a fixed inlet flowrate of 0.7 L min^{-1} and a HTF temperature of 3.5°C for freezing. After the solidification was completed, the melting was triggered by increasing the inlet temperature to 25°C, which took approx. 30 min to reach the set value. The temperature variations of three thermocouples in each of the six capsules during freezing and melting are shown in Figure 7 together with the tunnel inlet temperature.

From the temperature curves some tendencies were observed. In the freezing process, the temperature rise occurred in all the curves was due to the exothermal solidification. Due to the temperature gradient in the HTF tunnel, the high measuring point that is close to the HTF surface started solidification the last for most cases. The nucleus forming in the freezing phase induced a phase-change process that is very different from that of melting. The areas enveloped by the PCM temperature curves and HTF temperature curves in the freezing period were relevant to the lateral capsule cross-sectional area and mass of PCM at the measuring positions. Since the enthalpy of a system is an extensive property, it is extrapolated that the area beneath the curves can be used as an indicator for the enthalpy of solidification of PCM around these positions. Although not possible to accurately determine the enthalpy with the available data, the area under the curves can be used to estimate and compare the enthalpy of different capsules.

In the melting phase, the temperature profile has a sharp increase before phase change and then a flattening during the phase change and finally another rise upon completion of the phase change. The portion in the capsule that melts first is evidenced by the first occurrence of flattening temperature. The two triangular shapes (tetrahedron and pyramid) showed a short and slight temperature drop at the lowest measuring point. This is because the PCM near the bottom tips melted first, so the high density solid PCM at the centre sinks in low density liquid PCM, suddenly reducing the temperature at the bottom of the capsule.

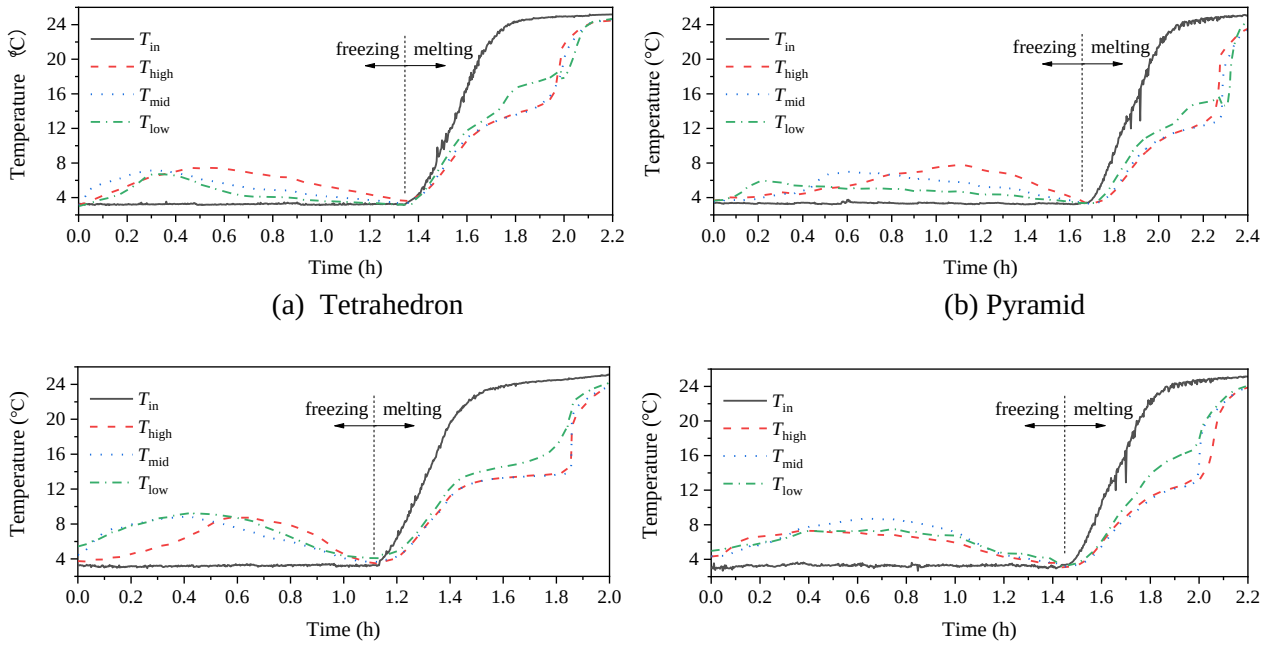

(a) Tetrahedron (b) Pyramid

(c) Tall cylinder (d) Short cylinder

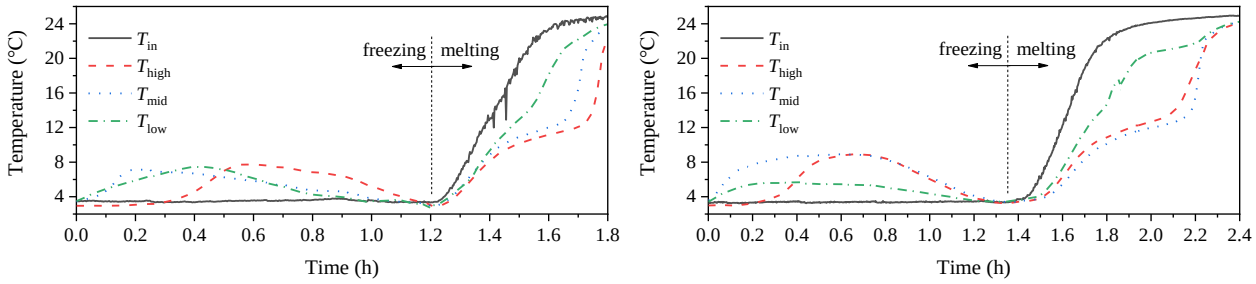

(e) RBC (f) Sphere

Figure 7. Capsule internal temperature variations during freezing and melting of different geometries, T_{in} indicates the inlet temperature of the tunnel, and T_{high}, T_{mid} and T_{low} represent the PCM temperature at the high, middle and low measuring point in the capsule.

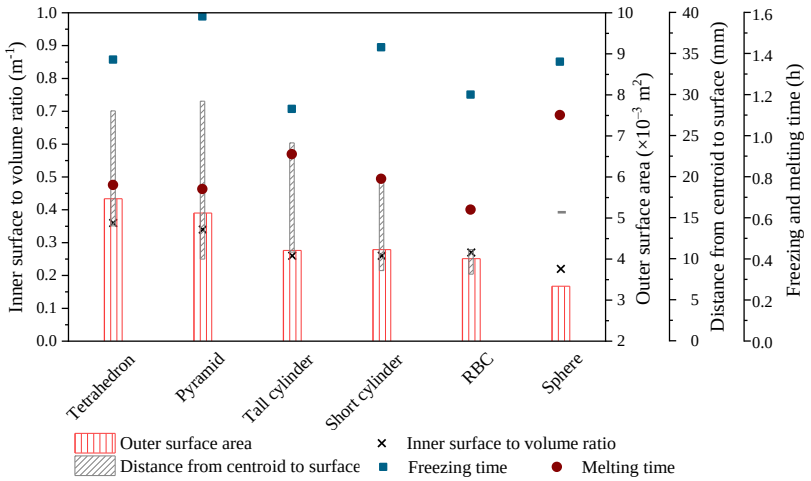

(a)

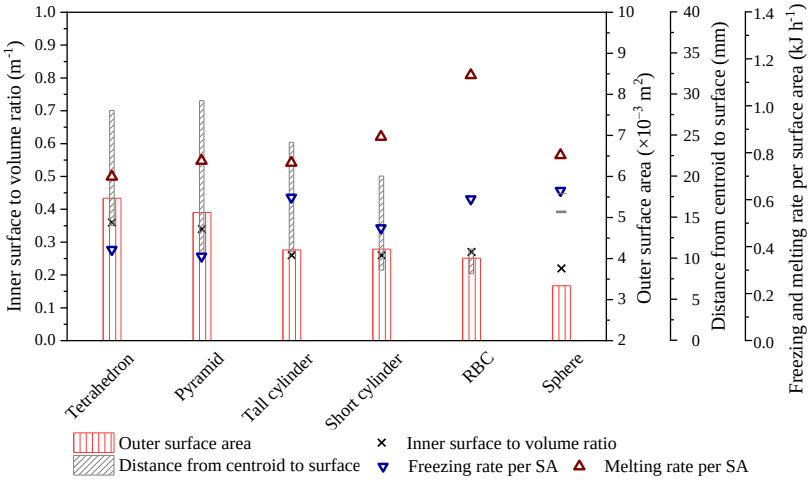

(b)

Figure 8. Key performance metrics of different geometries: (a) freezing and melting time, and (b) freezing and melting rate per surface area

The freezing and melting time, together with the freezing and melting rate per surface area are shown in Figure 8, with both the surface area and the distance range from centroid to inner surface of the six geometries. The distance from the centroid to surface is considered as the heat transfer distance and indicated by a range of existing values in Figure 8. The melting time in Figure 8(a) is defined as the time required for the entire encapsulated PCM to turn liquid and the centroid is the place where the last piece of solid persists for fixed melting. RBC is an exception, as its biconcave disc-shape with a dent on each side creates a very

short heat transfer distance. Therefore, the places with the last pieces of solid are the centres of the sectional annuli, as indicated in Figure 9. From Figure 8(a), the freezing time for tall cylinder and RBC was shorter (1.13 and 1.20 hours respectively). It is also seen that the freezing time of the two triangular shapes were in general longer (1.37 hours for tetrahedron and 1.58 hours for pyramid). The melting time of RBC was the shortest (0.64 hour), followed by pyramid (0.74 hour) and tetrahedron (0.76 hour). The melting time was affected by both the capsule surface area and the distance between the capsule centroid and the surface (i.e. the longest heat transfer distance).

The effect of the heat transfer distance on the melting process can be viewed from the melting time per surface area of each capsule geometry in Figure 8(b). In general, the shorter distance the higher the melting rate per surface area. The sphere, with the smallest surface area and large heat transfer distance (15.3 mm, the radius), had the longest melting time. Comparing the tall and the short cylinder with almost the same surface area (as per Table 2), due to the larger heat transfer distance, the tall cylinder had a much longer melting time. The shortest melting time was for the RBC-shaped capsule. Because of its shortest heat transfer distance together with a relatively large surface area, it achieved a melting time of 0.64 h, even shorter than that of tetrahedron and pyramid by 13.5%, despite them having larger surface areas. Regardless of the heat transfer surface area, the comparison conducted in the average freezing and melting rate per surface area in Figure 8(b) indicates an interesting trend: the larger the heat transfer distance (i.e. distance from centroid to surface), the lower the heat transfer rates per surface area. Importantly, the RBC was found to be the optimal geometry, corresponding to this trend. From Figure 8 the correlation of the freezing time/rate with the SA/V ratio and the heat transfer distance is not obvious, as it could be more relevant to other geometric features of the capsules, as discussed below in relation to the morphology study.

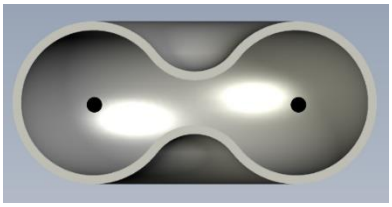

Figure 9. Cross-section view of RBC-shaped PCM capsule.

4.2 Morphology of phase change interface

In the freezing phase, the formation of seed nuclei and the growth of crystals happened slowly and therefore the freezing time was longer than the melting time. The tetrahedron and pyramid had the first solids appear at the tip (at the bottom) due to the small thermal mass in that region and a low temperature, which occurred probably due to a thin boundary layer that forms near the edges of the immersed capsule. The subsequent solidification was upward in only one direction, as shown in Figure 10 (a–d) and as a result they had the longest freezing time. In contrast, the first crystals in other capsules formed at the middle and grew towards both the top and the bottom, as shown in Figure 10(e–h), resulting in a faster freezing process. For these capsule shapes, where the thermal mass is uniform throughout the height of the capsule, nuclei had a larger growth rate where there was a surface to provide sites for nucleation. In this case, the thermocouple behaved as this surface. In addition, as solid hydrate particles have larger density than liquid PCM, this made the solidification in the downward direction more rapid, while the triangular shapes do not have this advantage. Besides, comparing the tall and the short cylinder, it is evidenced again that the vertical solidification is faster than the lateral solidification, as gravity assists in transporting and aggregating crystals in the vertical direction, as shown in Figure 8(a). Further studies on the effect of solid PCM transport during the freezing phase are needed to have a better understanding of the role of solid descent on the phase change.

The flow direction was from the right to the left. As can be seen in Figure 10(g), the solidified region reached the inner surface of the capsule on the side where the freestream flow is impinging. Unlike freezing, melting always proceeded from outer layers to inner layers, as indicated by the arrow in Figure 10(i), showing “Liquid” on the outer side and “Solid” on the inner side. Compared to freezing, which only underwent conduction in PCM, the melting process in the capsule included conduction as well as advection due to natural convection. The natural convection is thought to have further shortened the melting process.

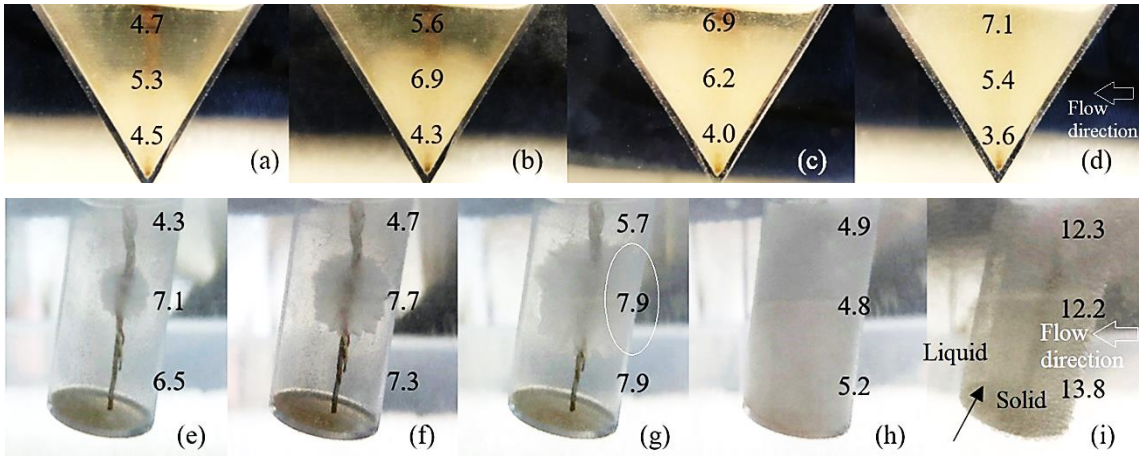

Figure 10. Appearance of capsules during phase change for the phases of (a–d) freezing in a pyramid at the time of 0.4, 0.8, 1.2 and 1.6 h from the beginning of solidification, (e–h) freezing in a long cylinder at the time of 0.2, 0.4, 0.6 and 0.8 h from the beginning of solidification, and (i) melting with the phase interface marked, with labelled temperature values in °C read from the thermocouples.

4.3 Influence of HTF flowrate and temperature

As the above experimental study showed the RBC shape to be the optimal geometry, the following investigation was conducted on the RBC-shaped capsule only. As shown in Figure 11, the effects of the HTF flowrate on the freezing time of capsule were studied at 1°C and 0.28, 0.70 and 1.2 L min^{-1}, respectively, and the effects on the melting time of capsule were studied at 25°C and 0.13, 0.9 and 1.4 L min^{-1}, respectively. The variation of freezing and melting time with the flowrate was approximately linear, as shown in Figure 11(a). The slope was –0.59 h per 1 L min^{-1} increment of flowrate for freezing and –0.25 h per 1 L min^{-1} increment for melting, revealing that the effect of HTF flowrate on the freezing process was more significant than that on the melting process. In average there was a 19.4% difference in the freezing time and a 22.0% difference in the melting time between two adjacent points.

The effects of HTF temperature on the freezing time of RBC-shaped capsule were studied at the flowrate of 0.70 L min^{-1} with the HTF set-point temperature of 1, 3 and 5°C, and those on the melting time were studied at 0.90 L min^{-1} with the HTF set-point temperature of 15, 20 and 25°C. The dependence of the freezing/melting time on HTF temperature was non-linear, as shown in Figure 11(b). The ratio of freezing time to HTF temperature increased with temperature; in contrast, the rate of melting time to HTF temperature dropped with temperature. This result reveals that there are optimal values of the HTF temperature which are likely to be close to 3°C for freezing and 20°C for melting.

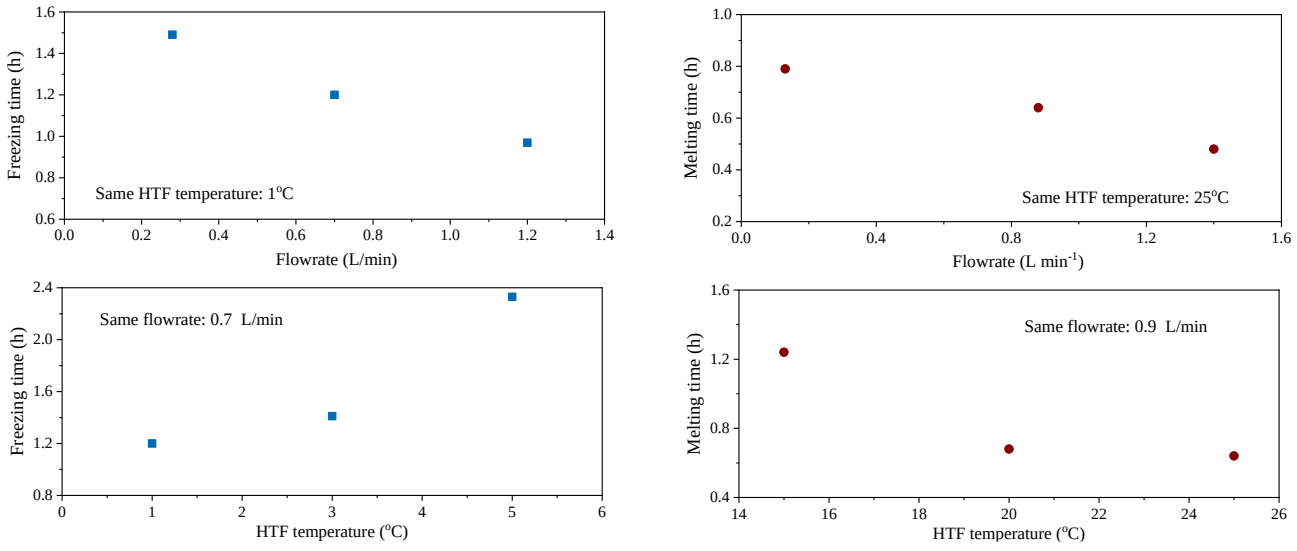

(a) (b)

Figure 11. Effects of HTF flowrate (a) and temperature (b) on freezing/melting time of a RBC-shaped capsule.

4.4 Influence of angle of attack

The effect of the angle of attack was studied in the HTF tunnel by adjusting the reference line (i.e. axis of symmetry) of the RBC-shaped capsule against the vertical plane normal to the freestream flow, for three orientations: vertical (90°; head-on), 45°, and horizontal (0°; crossflow), as illustrated in Figure 12. The temperature variation for the middle and lower thermocouples is shown in Figure 13 during freezing time. The freezing time of the three layouts differed significantly, with the horizontal configuration exhibiting the longest time (3.12 h) and the vertical configuration the shortest (1.17 h), as shown in Figure 14. Five mechanisms are thought to have contributed to this result.

(1) Heat transfer surface area. The impinged surfaced is larger for the capsule when it is vertical that results in stronger convection.

(2) Heat transfer mechanisms around the dent. The horizontal (crossflow) configuration is thought to have an HTF—warmer than the freestream—circulating within the dented region of the RBC, as in Ref. [17], so that the heat transfer between PCM and freestream flow is reduced, resulting in a longer freezing time.

(3) Natural convection inside the capsule. Natural convection occurs since the density of solid PCM is higher than that of liquid PCM. The results suggest that in a freezing phase, a capsule with a larger vertical dimension would favour the natural convection inside the PCM, thus helping accelerate the phase change process.

(4) Sedimentation of crystals. A longer descent distance of crystals resulted in a longer crystal suspending time. The total surface area of crystals is larger when they are suspended in liquid rather than in sediments, and a larger surface area enhanced heat transfer in the solidification.

(5) Chance of agglomeration of seed nuclei. The nucleation process has metastable phases persisting over long periods of time. Small fluctuations of the new stable phase tend to disappear while large fluctuations tend to grow [35]. Seed nuclei have to agglomerate into nucleation clusters to reach the size of critical nuclei so as to proceed to the growth period. A smaller transverse diameter is beneficial to increase the chance of agglomeration of seed nuclei to form the critical nuclei to complete nucleation.

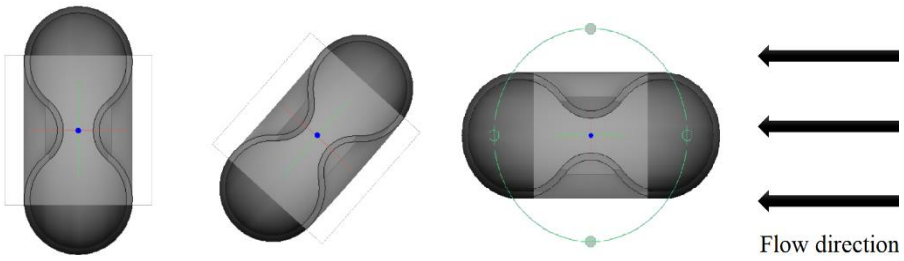

(a) (b) (c)

Figure 12. RBC-shaped capsule orienataions: (a) vertical (90°), (b) 45°, and (c) horizontal (0°).

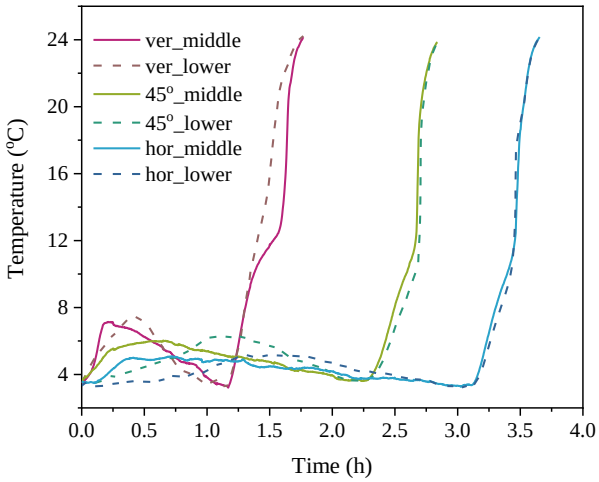

Figure 13. Temperature variations of RBC-shaped capsule with different tile angles during freezing time, in the labels “ver” means vertical and “hor” means horizontal orientation of the capsule.

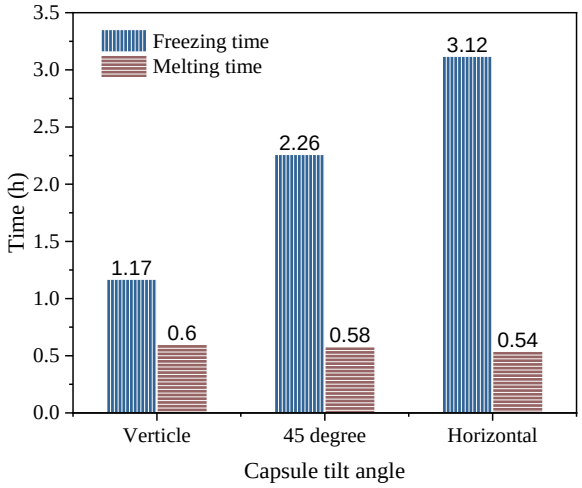

Figure 14. Effects of tile angle on freezing and melting time of RBC-shaped capsule

A previous finding showed that the crossflow is recommended for the RBC-shaped capsule layout in the CTES, due to its low drag force with a relatively high surface average Nusselt number [21]. This does not conflict with the present finding that the vertical capsule layout was the best. In fact, the literature focused on the properties of the external flow in terms of reducing pressure head in the hydraulic system and enhancing convective heat transfer; while the present work looked at the PCM freezing process which is affected by many other factors such as the gathering of seed nuclei and natural convection inside the capsule. On the other hand, the results of the melting process were in agreement with the previous study, in that the horizontal layout is most recommended as it led to the shortest melting time of 0.54 h. For the melting, SA/V is a main driving force. As a result, as can be seen in Figure 13, the difference in the melting of the three orientations was not significant due to the same geometry.

Another feature noticed was that the PCM temperature difference inside the capsule was smaller as the capsule was more horizontal, as shown in Figure 12. This can be seen especially from the melting process, during which the temperature of the middle and lower point inside the horizontal capsule was nearly the same. It is attributed to the fact that the temperature gradient in the water tunnel across the capsule is the largest for the vertical capsule and the smallest for the horizontal one.

5 Conclusions

This work looked at the heat transfer performances and phase change behaviours of six equal-volume varying-shape PCM capsules for use in cold latent heat storage through experimental methods. TBAB clathrate

hydrate was used as PCM in the current study. For potential practical applications, two typical cases were studied: (a) PCM capsule melting in air to estimate the performance PCM-embedded building envelopes under natural convection, and (b) PCM capsule freezing and melting in water to investigate the performance of PCM packed-bed CTES under forced convection. For the latter, the influence of the HTF temperature, flowrate and angle of attack for freezing and melting phases were studied. The main conclusions are as follows:

(1) The melting process was affected by both the capsule surface area and the distance between the capsule centroid and the inner surface of the capsule. Melting-in-air and freezing/melting-in-water experiments all showed that the RBC-shaped capsule had the best performance. RBC has a biconcave disc-shape with a dent on each side creating very short heat transfer distance. As a result, this shape was recommended as the optimal geometry for PCM capsules.
(2) The tetrahedron and pyramid had long freezing times as the first solid appeared at the tip due to the small thermal mass and low temperature. The subsequent solidification progressed in the upward direction. Crystallisation in other capsules occurred at the centre and then grew towards both the top and the bottom, resulting in a faster freezing process.
(3) For a surrounding flow in natural and forced convection regimes, both freezing and melting in a capsule with a larger vertical dimension was favoured. Different mechanisms contributed to the faster melting and freezing of vertically elongated shapes, including heat transfer surface area, heat transfer around the dent, natural convection inside the capsule, sedimentation of crystals, and chance of agglomeration of seed nuclei.
(4) The variation of freezing and melting time with the HTF flowrate was approximately linear, whereas the effect of the freestream temperature on the phase change was non-linear. Optimal values of the HTF temperature were likely to be close to 3°C for freezing and 20°C for melting.
(5) The freezing time of the RBC-shaped capsule with different angles of attack was significantly different, with the vertical capsule in a head-on configuration with the freestream flow showing the shortest freezing time. This configuration is recommended for capsule layouts.

Abbreviation

AC	air conditioning
CTES	cold thermal energy storage
HTF	heat transfer fluid
IR	infrared
PCM	phase change material
RBC	red blood cell
SA/V	surface area to volume
TBAB	tetra-*n*-butylammonium bromide

Reference

[1] D. Ürge-Vorsatz, L. F. Cabeza, S. Serrano, C. Barreneche, and K. Petrichenko, "Heating and cooling energy trends and drivers in buildings," *Renewable and Sustainable Energy Reviews*, vol. 41, pp. 85–98, Jan. 2015

[2] I. Sarbu and C. Sebarchievici, "A comprehensive review of thermal energy storage," *Sustainability*, vol. 10, no. 1, p. 191, Jan. 2018

[3] X. Wang and M. Dennis, "A comparison of battery and phase change coolth storage in a PV cooling system under different climates," *Sustainable cities and society*, vol. 36, pp. 92–98, 2018

[4] X. Wang and M. Dennis, "Influencing factors on the energy saving performance of battery storage and phase change cold storage in a PV cooling system," *Energy and Buildings*, vol. 107, pp. 84–92, 2015

[5] M. Esen and T. Ayhan, "Development of a model compatible with solar assisted cylindrical energy storage tank and variation of stored energy with time for different phase change materials," *Energy Conversion and Management*, vol. 37, no. 12, pp. 1775–1785, 1996

[6] M. Esen, A. Durmuş, and A. Durmuş, "Geometric design of solar-aided latent heat store depending on various parameters and phase change materials," *Solar Energy*, vol 62, no. 1, pp. 19–28, 1998

[7] M. Esen, "Thermal performance of a solar-aided latent heat store used for space heating by heat pump," *Solar Energy*, vol 69, no. 1, pp. 15–25, 2000

[8] X. Jia, X. Zhai, and X. Cheng, "Thermal performance analysis and optimization of a spherical PCM capsule with pin-fins for cold storage," *Applied Thermal Engineering*, vol. 148, pp. 929–938, Feb. 2019

[9] Y. E. Milián, A. Gutiérrez, M. Grágeda, and S. Ushak, "A review on encapsulation techniques for inorganic phase change materials and the influence on their thermophysical properties," *Renewable and Sustainable Energy Reviews*, vol. 73, pp. 983–999, Jun. 2017

[10] P. Chandrasekaran, M. Cheralathan, and R. Velraj, "Influence of the size of spherical capsule on solidification characteristics of DI (deionized water) water for a cool thermal energy storage system – An experimental study," *Energy*, vol. 90, pp. 807–813, Oct. 2015

[11] A. Raul, M. Jain, S. Gaikwad, and S. K. Saha, "Modelling and experimental study of latent heat thermal energy storage with encapsulated PCMs for solar thermal applications," *Applied Thermal Engineering*, vol. 143, pp. 415–428, Oct. 2018

[12] X.Q. Zhai, X.L. Wang, T. Wang, R.Z. Wang, "A review on phase change cold storage in air-conditioning system: Materials and applications," *Renewable and Sustainable Energy Reviews*, vol. 22, pp. 108–120, Jun. 2013

[13] X. Kong, L. Wang, H. Li, G. Yuan, and C. Yao, "Experimental study on a novel hybrid system of active composite PCM wall and solar thermal system for clean heating supply in winter," *Solar Energy*, vol. 195, pp. 259–270, Jan. 2020

[14] E. Meng, J. Wang, H. Yu, R. Cai, Y. Chen, and B. Zhou, "Experimental study of the thermal protection performance of the high reflectivity-phase change material (PCM) roof in summer," *Building and Environment*, vol. 164, p. 106381, Oct. 2019

[15] S. H. Choi, J. Park, H. S. Ko, and S. W. Karng, "Heat penetration reduction through PCM walls via bubble injections in buildings," *Energy Conversion and Management*, vol. 221, p. 113187, Oct. 2020

[16] J. F. Torres, F. Ghanadi, I. Nock, M. Arjomandi, and J. Pye, "Mixed convection around a tilted cuboid with an isothermal sidewall at moderate Reynolds numbers," *International Journal of Heat and Mass Transfer*, vol. 119, pp. 418–432, Apr. 2018

[17] J. F. Torres, F. Ghanadi, Y. Wang, M. Arjomandi, and J. Pye, "Mixed convection and radiation from an isothermal bladed structure," *International Journal of Heat and Mass Transfer*, vol. 147, p. 118906, Feb. 2020

[18] R. I. ElGhnam, R. A. Abdelaziz, M. H. Sakr, and H. E. Abdelrhman, "An experimental study of freezing and melting of water inside spherical capsules used in thermal energy storage systems," *Ain Shams Engineering Journal*, vol. 3, no. 1, pp. 33–48, Mar. 2012

[19] R. M. Reddy, N. Nallusamy, and K. H. Reddy, "The effect of PCM capsule material on the thermal energy storage system performance," *ISRN Renewable Energy*, 2014

[20] F. Benmoussa, A. Benzaoui, and H. Benmoussa, "Thermal behaviour of latent thermal energy storage unit using two phase change materials: Effects of HTF inlet temperature," *Case Studies in Thermal Engineering*, vol. 10, pp. 475–483, Sep. 2017

[21] X. Cheng, X. Zhai, X. Wang, and P. Lin, "Numerical study of forced convection over phase change material capsules in a traditional spherical shape and a biomimetic shape," *Journal of Energy Storage*, vol. 31, p. 101526, Oct. 2020

[22] X. Cheng and X. Zhai, "Thermal performance analysis of a novel PCM capsule in red blood cell shape," *Applied Thermal Engineering*, vol. 120, pp. 130–137, Jun. 2017

[23] A. A. Rabienataj Darzi, M. Jourabian, and M. Farhadi, "Melting and solidification of PCM enhanced by radial conductive fins and nanoparticles in cylindrical annulus," *Energy Conversion and Management*, vol. 118, pp. 253–263, Jun. 2016

[24] A. Awasthi, B. Kumar, H. H. Nguyen, S. S. Lee, and J. D. Chung, "Effect of sinusoidal cylindrical surface of PCM on melting performance," *J Mech Sci Technol*, vol. 34, no. 8, pp. 3395–3402, Aug. 2020

[25] M. Hlimi et al., "Melting inside a horizontal cylindrical capsule," *Case Studies in Thermal Engineering*, vol. 8, pp. 359–369, Sep. 2016

[26] Autex. 2020. "3D Tiles". [online] Available at: <https://www.autexglobal.com/au/acoustic-products/3d-tiles/> [Accessed 30 November 2020].

[27] X. Wang, M. Dennis, J. Jiang, L. Zhou, X. Zhai, and W. Lipiński, "Performance of a novel cold thermal storage material in an emulated air conditioning system using different storage strategies," *International Journal of Refrigeration*, vol. 104, pp. 259–269, 2019

[28] X. Wang, X. Zhai, H. Zhang, and L. Zhou, "A theoretical and experimental study of a TBAB salt hydrate based cold thermal energy storage in an air conditioning system," *Thermal Science and Engineering Progress*, vol. 13, pp. 100397, 2019

[29] X.J. Shi and P. Zhang, "Cold storage by tetra-n-butyl ammonium bromide clathrate hydrate slurry generated with different storage approaches at 40 wt% initial aqueous solution concentration," *International Journal of Refrigeration*, vol. 42, pp. 77–89, 2014

[30] X. Wang and M. Dennis, "An experimental study on the formation behavior of single and binary hydrates of TBAB, TBAF and TBPB for cold storage air conditioning applications," *Chemical Engineering Science*, vol. 137, pp. 938–946, 2015

[31] H. Hashemi, S. Babaee, A. H. Mohammadi, P. Naidoo, and D. Ramjugernath, "State of the art and kinetics of refrigerant hydrate formation," *International Journal of Refrigeration*, vol. 98, pp. 410–427, Feb. 2019

[32] H. Oyama et al., "Phase diagram, latent heat, and specific heat of TBAB semiclathrate hydrate crystals," *Fluid Phase Equilibria*, vol. 234, no. 1, pp. 131–135, Jul. 2005

[33] T. Asaoka, H. Kumano, and M. Serita, “Measurement of latent heat of tetra-*n*-butylammonium bromide (TBAB) hydrate,” *International Journal of Refrigeration*, vol. 36, no. 3, pp. 992–997, May 2013

[34] K. Fujiura, Y. Nakamoto, Y. Taguchi, R. Ohmura, and Y. Nagasaka, “Thermal conductivity measurements of semiclathrate hydrates and aqueous solutions of tetrabutylammonium bromide (TBAB) and tetrabutylammonium chloride (TBAC) by the transient hot-wire using parylene-coated probe,” *Fluid Phase Equilibria*, vol. 413, pp. 129–136, Apr. 2016

[35] S. Sakrani, L. Jie, and W. Yussof, “The formation of nanoscale clusters - nanofilms / quantum dots predicted using a capillary model of nucleation,” *Malaysian Journal of Fundamental and Applied Sciences*, vol. 1, Jan. 2008